Infectious Disease Modelling 2 (2017) 90–99

Contents lists available at ScienceDirect

Infectious Disease Modelling

journal homepage: www.keaipublishing.com/idm

Modelling the HIV persistence through the network of lymphocyte recirculation in vivo

Ying Huang [a], Chen Zhang [b], Jianhong Wu [c], Jie Lou [a, *]

[a] Department of Mathematics, Shanghai University, 99 Shangda Road, Shanghai 200444, PR China
[b] 2525 West End Ave. Suite725, Nashville, TN, 37215, Vanderbilt Institute for Global Health at Vanderbilt Medical Center, USA
[c] MITACS Centre for Disease Modeling, York University, Toronto, Ontario, M3J 1P3, Canada

ARTICLE INFO

Article history:
Received 22 December 2016
Received in revised form 22 February 2017
Accepted 23 February 2017
Available online 28 February 2017

2010 MSC:
39A11
92D30

Keywords:
HIV reservoirs
Blood-brain barrier
Dynamical model
Lymphocyte recirculation network

ABSTRACT

Human Immunodeficiency Virus (HIV) is able to persist in cellular and/or anatomical viral reservoirs, despite the effective inhibition of virus replication by the antiretroviral therapy (ART). Here we develop a mathematical model to gain some insights of HIV persistence relevant to the lymphocyte recirculation network of immune system and the central nervous system (CNS). Our simulations and analyses illustrate the role of the CNS as a virus reservoir to prevent antiretroviral drugs from penetrating the blood-brain (or blood-testis) barrier, and we examine the long-term impact of this reservoir on the transmissibility of an infected individual. We observe numerically that level of HIV in peripheral blood may not accurately reflect the true mechanisms occurring within other organs.

1. Introduction

1.1. The immune system and lymphocyte recirculation

The immune system protects the human body against diseases or any potentially threatening foreign bodies (e.g., virus, bacteria and parasites). The immune system operates throughout the body. However, there are certain sites where the cells of the immune system are organized with specific structures, classified as the central lymphoid tissue (e.g., bone marrow, thymus) and peripheral lymphoid tissues (e.g., lymph nodes, spleen, mucosa-associated lymphoid tissue). There are about 600–700 lymph nodes present in the human body. Lymphocytes can recirculate between lymphoid and non-lymphoid tissues, which allows lymphocytes to fight against antigens. The lymphocytes is valuable in distributing effector cells among sites where they are needed. The recirculation is a complex process as shown in (Sae-Jang,), where recirculation involves the procedure of a precursor pool of uncommitted lymphocytes from the blood into lymph nodes or mucosal lymphatic tissues and then moves back to the blood again, forming the basis of immuno-surveillance and integration of immune functions across the segregated systems. Activated lymphocytes move from the spleen and lymph nodes into the

* Corresponding author.
E-mail address: jie.lou@126.com (J. Lou).
Peer review under responsibility of KeAi Communications Co., Ltd.

http://dx.doi.org/10.1016/j.idm.2017.02.003

blood as well as other lymphoid and non-lymphoid tissues. Enough lymphocytes recirculation from the lymph to blood can replace the total blood lymphocyte pool from 10 to 48 times every 24 h.

1.2. HIV in blood, tissues and reservoirs

Persistent low-level viremia is a common feature among HIV patients treated with highly active antiretroviral therapy (HAART) (Levy, 1995). An important research question to address is whether residual viremia can lead to ongoing cycles of viral replication even under HAART, or it signifies a release of virus from stable reservoirs infected before the initiation of therapy. Several reports have shown that no viral evolution happened among treated patients (Bailey et al., 2006; Nottet et al., 2009; Persaud et al., 2004), indicating that ART can completely stop viral replication at least among some patients (Shen & Siliciano, 2008). In a study among patients who discontinued drugs during the structured treatment interruptions (STI) therapy, these rebounding virus resembled pretreatment virus, and did not show any evidence of genetic evolution over time (Joos et al., 2008). The lack of new resistance mutations detected in patients on ART with suppressed plasma viremia (less than 50 copies/ml) further argues against ongoing viral replication, implying the release of virus from stable cellular reservoirs as an important source for residual viremia (Nettles et al., 2005; Nottet et al., 2009; Persaud et al., 2004). Virus isolated from resting memory $CD4^+$ T-cells has been shown to be closely related to residual plasma virus that found among patients with ongoing ART, thus indicating the latent reservoir as a source of residual viremia in these patients (Bailey et al., 2006; Nottet et al., 2009; Persaud et al., 2004; Shen & Siliciano, 2008). Latently infected resting memory $CD4^+$ T-cells can persist for years (half-life, 44 months), which represent a major barrier to HIV eradication. Removal of HIV from these resting memory $CD4^+$ T-cells or other reservoirs of other tissues (e.g., the brain) could take considerably longer or even be unattainable (Levy, 1995).

HIV virions are produced by infected cells in both lymphoid tissues and blood (Haase et al., 1996; Perelson et al., 1997). Because of a great concern for the reported HIV transmission by blood, major efforts have been made earlier to quantify the amount of virus in blood. The results indicated that both freely-flowed virus and infected cells were present in blood regardless if the HIV-infected individual is asymptomatic or develops AIDS (Levy, 1995). However, in many cases, the level of freely-flowed virus in the peripheral blood, even following antiviral therapy, may not give an accurate reflection of what is occurring within the body (Levy, 1995). For instance, the study (Ping et al., 2000) reported that the quantity of HIV in blood plasma may not reflect the level of semen viremia. Researchers (Tachet et al., 1999) also found a small group of men had RNA levels in seminal plasma comparable to or even higher than that detected in blood plasma (Levy, 1995). Other literature also revealed that virus can be detected in semen by cell culture or PCR techniques despite antiviral therapy when plasma virus levels were low or undetectable (Hamed, Winters, Holodniy, Katzenstein, & Merigan, 1993; Vernazza et al., 1994). These findings indicate the inability of some drugs to penetrate the blood-testis barrier and emphasize the transmissibility of an infected person despite low viremia levels (Barker & Billingham, 1997; Levy, 1995).

Like what has happened in testis, HIV has also been readily isolated, even in early infection, from the central nervous system (CNS). About a quarter of AIDS patients have neurologic symptoms, particularly the HIV encephalitis, which can occur despite the use of HAART (Levy, 1995). In contrast to these body fluids, cerebrospinal fluid (CSF) contains large amounts of virus, particularly in individuals with neurologic findings. It can be present in the CSF of asymptomatic individuals (Ho et al., 1985; Levy, 1995; Levy, Hollander, Shimabukuro, Mills, & Kaminsky, 1985). Simultaneous comparison of viral RNA sequences in CSF and plasma samples have indicated that the differences that support the conclusion that the brain is a distinct compartment particularly within the choroid plexus (Burkala, He, West, Wood, & Petito, 2005; Tang, Huong, Lloyd, Spearman, & Haas, 2000). The mechanism(s) by which HIV enters the CNS is not known, but entry occurs obviously among freely-flowed virus or among infected cells. Activated infected cells enter the CNS by attachment and diapedesis between endothelial cells (Hickey, Hsu, & Kimura, 1991). Both types of peripheral blood cells (macrophages and $CD4^+$ T-cells) could, therefore, be the initial source of HIV infection, although in vitro studies suggest that infected CD4 lymphocytes preferentially migrate to the brain through the endothelium (Birdsall et al., 1997). Similarly, freely-flowed virus can readily enter the CSF and brain from the blood via the vascular endothelium (Davis et al., 1992).

2. The model

Insights into HIV dynamics in vivo have been obtained from mathematical modelling (see e.g., (Nowak & May 2001; Perelson & Nelson, 1999)). Competition models have been formulated in the context of the dynamics of virus-host interactions in the past two decades (Frost & McLean, 1994; Korthals Altes and.Jansen, 2000; McLean & Nowak, 1992; Rong, Feng, & Perelson, 2007; Smith & Wahl, 2004, 2005; Wahl & Nowak, 2000). These models embedded the knowledge on the possible dynamics of HIV-1 infection into relatively complex systems of non-linear differential equations. Such results can be used, for example, to investigate different hypotheses on HIV dynamics through numerical simulations. In (Callaway & Perelson, 2002) authors examined the predictability of several biologically oriented models of HIV-1 dynamics to explain sustained low viral loads. They built a chronically infected cell model by considering the infection stages occurring in two distinct compartments, with one regarded as a drug sanctuary, such as the brain, or testis. These compartments are then coupled by allowing the transportation of virus between these compartments. Authors permitted virus transporting between the main compartment and the sanctuary. Considering the lymphocyte recirculation, our model is a modified version of this

virus dynamics model (Callaway & Perelson, 2002) with specific considerations of the network of different lymphoid tissues, blood and the HIV sanctuary, such as the testis and the brain/CNS in vivo.

The model is formulated as follows. In organ i (it can be a tissue, blood, the testis or the brain), T_i represents CD4$^+$ T cells that are susceptible to infection, T_i^* productively infected cells, C_i^* chronically infected cells and V_i viral load. The following equations represent the rates of change of these populations under the effect of ART:

$$\begin{cases} \dfrac{dT_i}{dt} &= \lambda_i - \omega T_i - (1-\varepsilon_i)kT_iV_i + \sum_{j=1}^{n} d_{ij}^{T} T_j A_{ij}, \\ \dfrac{dT_i^*}{dt} &= (1-\alpha_i)(1-\varepsilon_i)kT_iV_i - \delta T_i^* + \sum_{j=1}^{n} d_{ij}^{T^*} T_j^* A_{ij}, \\ \dfrac{dC_i^*}{dt} &= \alpha_i(1-\varepsilon_i)kT_iV_i - \mu C_i^* + \sum_{j=1}^{n} d_{ij}^{C^*} C_j^* A_{ij}, \\ \dfrac{dV_i}{dt} &= N_T\delta T_i^* + N_C\mu C_i^* - \sigma V_i + \sum_{j=1}^{n} d_{ij}^{V} V_j A_{ij}, \end{cases} \tag{1}$$

where $i = 1, 2, \ldots, n$. We organize the model in such a way that compartment $i = 1$ represents the blood system; compartment $i = n$ represents the CNS and rest represents other tissues such as lymph nodes, spleen and mucosa-associated lymphoid tissue.

In model (1), the constant λ represents a source of susceptible cells, and ω is their death rate. k is the infection rate, and infection is assumed to occur at a rate proportional to the product of the concentration of virus and target cells, an assumption which is valid for a well-mixed system with relatively high concentrations of each product. A fraction α of the infection events result in chronic infections, chronically infected cells die with a rate μ. δ is the infected cell death rate, N_T and N_C are the average number of virions produced in the lifetime of short-lived and chronically infected cells, respectively and σ is the rate at which free virus is cleared. RT inhibitors prevent HIV RNA from being converted into DNA, a crucial part of the viral life cycle. Thus, the infectiousness of the virus, k, is reduced by the quantity $(1-\varepsilon)$, where ε represents the efficacy of RT inhibitors and $0 \le \varepsilon \le 1$. The dispersal of cells and virus among blood, tissues and the sanctuary (such as the brain) are governed by the rate constants d^T, d^{T^*}, d^{C^*} and d^V. The details of these parameters can be found in the Appendix.

3. Results and discussion

First, we calculated the basic reproduction number R_0 in terms of model parameters using the "next-generation operator" method (Van den Driessche and.Watmough, 2002), which can be found in the Appendix. Also, we predicted the effectiveness of ART in HIV positive individuals with some numerical and uncertainty analyses. Since the values of most parameters are less certain in different individuals, we used Latin hypercube sampling (Blower, Gershengorn, & Grant, 2000), a type of stratified Monte Carlo sampling, for each of the uncertainty parameter. We assigned each uncertain parameter a probability density function (pdf), to reflect either the uncertainty in the value of the parameter, or the degree to which the parameter could vary if it was being used as an "experimental variable". By perturbing these parameters, we investigated their influences on estimates of R_0 and therapy effect. The uncertainty ranges of all universal parameters and their literature are shown in Table 1.

Table 1
Parameters.

Para	Meaning	Range	Distribution	Reference
λ	source of susceptible cells	$(0, 40)$	Triangular	(Lou, Lou, & Wu, 2002)
ω	death rate of susceptible cells	$(0.01{*}0.75, 0.01, 0.01{*}1.25)$	Triangular	(Callaway & Perelson, 2002)
δ	death rate of infected cells	$(0.7{*}0.75, 0.7, 0.7{*}1.25)$	Triangular	(Callaway & Perelson, 2002)
ε	efficacy of ART in blood, tissues and the brain			(Callaway & Perelson, 2002)
k	infection rate	$(0, 0.00001, 0.001)$	Triangular	(Callaway & Perelson, 2002)
α	fraction result in chronic infection	$(0.159{*}0.75, 0.159)$	Triangular	(Callaway & Perelson, 2002)
μ	the chronically infected cell decay rate	$(0.7/5{*}0.75, 0.7/5, 0.7/5{*}1.25)$	Triangular	(Callaway & Perelson, 2002)
N_T	number of virions produced by a short-lived infected cells	$(1, 100, 200)$	Triangular	(Callaway & Perelson, 2002)
N_C	number of virions produced by a long-lived infected cells	$(1{*}0.1, 100{*}0.1, 200{*}0.1)$	Triangular	(Callaway & Perelson, 2002)
σ	rate at which free virus is cleared	$(1, 3, 10)$	Triangular	(Lou et al., 2002)
d_{ij}	transport rate of cells and virus among blood and tissues	$(0.05, 0.2)$	Constant	(Callaway & Perelson, 2002)
d_{ij}	transport rate of cells and virus between blood and the brain	$(0.005, 0.02)$	Constant	(Callaway & Perelson, 2002)
T	initial value of T cells	$(50, 800)$	Constant	Estimated
T^*	initial value of infected T cells	$(5, 50)$	Constant	Estimated
C^*	initial value of chronically infected cells	$(1, 25)$	Constant	Estimated
V	initial value of HIV-1 virus	$(1, 1000)$	Constant	Estimated

Especially, chronically infected cells contribute to at least 1% of the total steady state viral load (Callaway & Perelson, 2002), here we suppose $N_C = N_T \times 0.1$. In the following simulations, we suppose the total number of tissues in the body is 600, ie., $n = 600$. We use a total of 500 Latin hypercube samplings in our simulations. For each Latin hypercube sampling, we consider four possible scenarios of ART (see Table 2):

Scenario A-No ART scenario: Under this scenario, we suppose the individual does not accept ART ($\varepsilon = 0$) for all organs and tissues in vivo.

Scenario B-Indiscriminate ART scenario: Under this scenario, we set $\varepsilon = 1$ (i.e. the drug efficacy are 100% and viral replication is completely inhibited) for all organs and tissues, including the Brain. That is, we suppose all organs are the same and do not consider the existence of the blood brain barrier (BBB).

Scenario C-High ART effect scenario: Under this scenario, we set $\varepsilon = 1$ (i.e. the drug efficacy are 100% and viral replication is completely inhibited) for blood and all lymphoid tissues. But for the brain, we randomly chosen ε in the range $(1/20, 1/10)$ for each simulation, considering the existence of the BBB.

Scenario D-Low ART effect scenario: Under this scenario, we set ε ranges in $[0.7, 1]$ (i.t., the drug efficacy are randomly chosen in 70%–100%) for blood and all lymphoid tissues in each Latin hypercube sampling. For the brain, we randomly choose ε in the range $[0.7/20, 1/10]$ for each simulation, considering the existence of the BBB.

3.1. Numerical and sensitivity analyses

We have a total of 500 realizations in our simulations. Under the uncertainty ranges of all universal parameters that shown in Table 1 and the four different scenarios, the distribution of the basic reproduction number R_0 is shown in Table 3. We show the mean and the media of R_0; the standard deviation [SD]; 95% confidence interval [CI]; and interquartile range [IQR], respectively in Table 3. Fig. 1 gives a visual graphic about the distribution of R_0.

Obviously, $R_0 = 0 < 1$ under scenario B is essentially different from the other three scenarios, which is not plotted here. This means, HIV virus can be eliminated from vivo under a high effect ART if we look the Brain the same as other organs or tissues. One interesting thing is: the distributions of R_0 have not big differences among the other three scenarios (Fig. 1 and Table 3). The mean values of R_0 of all of the other three scenarios are much higher than 1, even if under the most effective ART treatment (Scenario C). This hints that ART can not eliminate HIV virus because of the existence of the BBB.

3.2. Predictions and uncertainty estimations

We compare the media concentrations of the 500 simulations under Scenario C and Scenario D (shown in Fig. 2). Healthy T cells (T), infected T cells (T^*), chronically infected cells (C^*) and HIV RNA (V) after ART (beginning at $t = 0$ days) in the Blood, the Brain and one Tissu (randomly selected among the total 600 tissues) respectively. The limit of detection for standard HIV-1 assays is 50 copies ml^{-1} (Callaway & Perelson, 2002).

We observe that healthy T cells (T) show slowly increasing in the blood and tissues under the both scenarios (Fig. 2 A), but these T cells first decay and then increase in the Brain. Obviously for each scenario, the levels of T cells in tissues is the highest and that in the Brain is the lowest after ART. This result indicates that, the concentration of healthy T cells (T) in Blood cannot represent the level in other tissue or organs.

HIV RNA (V) decays fast after ART initiation under the two scenarios for all the three organs (Fig. 2 D). After about two weeks, the concentrations of HIV RNA (V) of almost all organs decay below the detection limit, even under Scenario D. But for the situation in the Brain, the trend is different. It has a slight fluctuation and then stable at about 280 copies ml^{-1}, which is much higher than that in the blood and tissues. The trends of HIV virus are almost the same between Scenario C and Scenario D in the CNS, which show that ART has not big effect on the virus located in the CNS. These results indicate that, even if the blood seems completely "cleaned" by ART, the Brain still reserves stable/transmissible HIV virus. From this perspective, we can call the CNS as a HIV virus "reservoir".

The concentrations of the infected T cells (T^*) and the chronically infected cells (C^*) show similar trends (Fig. 2B and C). An obvious difference is that the concentration of C^* has a much slower decay trend compare to T^*. This observation indicates that these long-lived chronically infected cells can be another kind of virus "reservoir". In both Scenario C and Scenario D, the concentration of HIV virus are higher in the Brain than that in the blood and tissues. These results again support that the CNS is actually a stable reservoir of HIV virus.

Fig. 3 gives us some idea about what happens in the Brain under Scenario B and Scenario C respectively. We show only the outcomes of the total infected T cells ($T^* + C^*$) and HIV virus (V) here. Each box-plot represents the results of 500 simulations. These plots show median values, upper and lower quartiles, and outlier cutoffs. In Fig. 3A, the concentrations of the total

Table 2
Predicting assumptions.

	Scenario A	Scenario B	Scenario C	Scenario D
In Blood	$\varepsilon = 0$	$\varepsilon = 1$	$\varepsilon = 1$	$\varepsilon \in [0.7, 1]$
In Tissues	$\varepsilon = 0$	$\varepsilon = 1$	$\varepsilon = 1$	$\varepsilon \in [0.7, 1]$
In the Brain	$\varepsilon = 0$	$\varepsilon = 1$	$\varepsilon \in [1/20, 1/10]$	$\varepsilon \in [0.7/20, 1/10]$

Table 3
Summary statistics of $\mathbf{R_0}$ under four different scenarios.

R_0	Scenario A	Scenario B	Scenario C	Scenario D
Mean	1.99	0	1.604	1.631
Media	1.907	0	1.545	1.578
SD	0.809	0	0.564	0.551
95% CI	1.89–2.09	0	1.532–1.677	1.559–1.703
IQR	1.45–2.29	0	1.217–1.926	1.212–1.935

infected T cells are shown. The black-triangle-line is the median line of the total 500 simulations of Scenario C. As a comparison, the blue-dot-line is the median line of Scenario B. Similarly, the red-triangle -line is the median line of Scenario C and the peach-dot-line is that of Scenario B of the concentration of HIV virus. Obviously, there are essential differences between the two assumptions. This again indicates that the importance of modelling based upon the biological basis.

Analyses of changes in virus load after initiation of treatment with potent antiretroviral agents has provided substantial insight into the dynamics of HIV-1. The concentration of HIV-1 in plasma drops by 99% in the first two weeks of treatment owning to the rapid elimination of free virus with a half-life of less than 6 h and loss of productively infected cells with a half-life of 1.6 days (Perelson, Neumann, Markowitz, Leonard, & Ho, 1996). In a study (Perelson et al., 1997), eight HIV infected patients who were naive to ART were recruited. *De novo* HIV replication in the patients was blocked by ART. After treatment was started, the HIV RNA concentration in plasma was measured in frequency using the branched DNA assay. Each patient responded to a similar pattern of viral decay: an initial rapid exponential decline (first phase), followed by a slower exponential decline (second phase). In addition, no infectious HIV was detectable in 10^7 peripheral blood mononuclear cells (PBMC) from each of the patients after 8 weeks of treatment. Our model simulations find a similar tendency, see Fig. 2 (B, C and D). In particular, in Fig. 2 D, the decays of HIV RNA have a clearly initial rapid exponential decline (first phase), followed by a slower exponential decline (second phase) in blood, in the CNS and also in all tissues. Obviously, the antiretroviral effect was potent in that plasma viraemia in patients dropped below the standard detection threshold of 50 copies ml^{-1} by 2 weeks of treatment in both blood and tissues. The situation in the CNS is however different, where HIV RNA concentration keeps at a stably and high level (about 272 copies ml^{-1} by media) even after two months!

4. Conclusion

We have developed a compartmental model for the HIV spread dynamics through the network of lymphocyte recirculation in vivo, to gain insights of HIV persistence in patients receiving highly effective ART. Our simulations agree well with previously documented observation of “initial rapid exponential decline” followed by a “slower exponential decline”, and thus confirm that antiretroviral effect can be potent in that plasma viraemia in patients can drop below the standard detection threshold after several weeks of treatment. Our simulations however clearly illustrate the significant role of the CNS as a reservoir in HIV persistence. In particular, we have shown that without consideration of the role of the CNS, the basic reproduction number R_0 can be reduced to below the unity, while incorporating the CNS in the model results in the R_0 value exceeding the unity even under an effective ART. We also note that in our designed simulations, the concentration of the HIV RNA is almost all regions decay to below the level of detection by standard HIV-1 assays, but the concentration of the HIV RNA in the CNS reaches a stable (after some transient fluctuation) level, much higher than that in the blood and tissues.

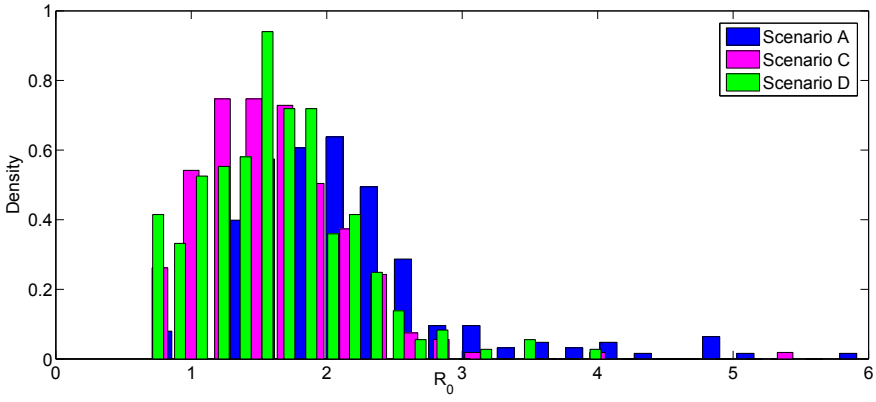

Fig. 1. The basic reproduction number R_0 under four different scenarios respectively.

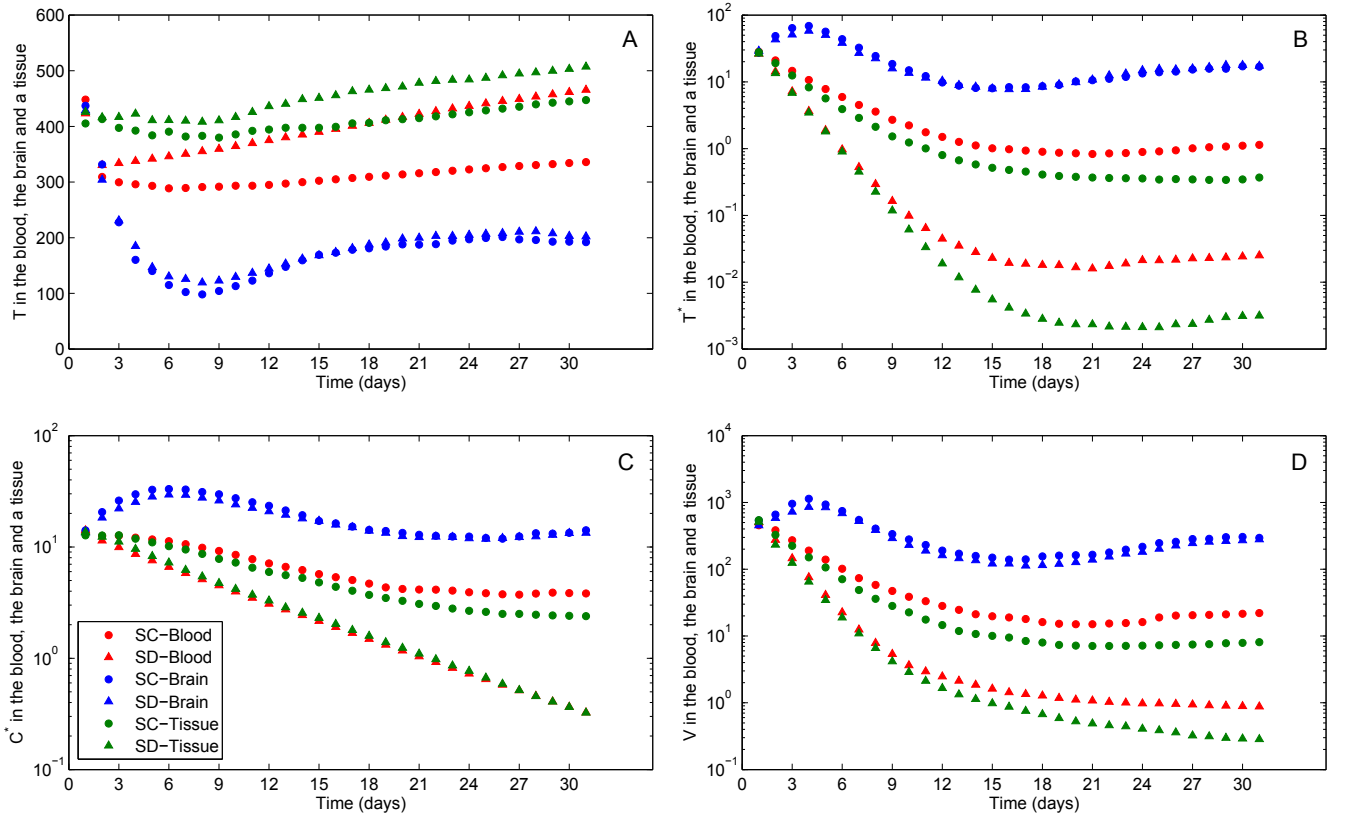

Fig. 2. The media concentrations of variables (healthy T cells (T), infected T cells (T^*), chronically infected cells (C^*) and HIV (V)) of 500 simulations under two scenarios respectively in the Blood, the Brain and one Tissue with system (1), beginning at $t = 0$ days. The detection threshold of HIV virus is 50 copies ml^{-1}. In the legend, SC-Blood means scenario C in the blood and SD-Brain means scenario D in the Brain, and so on.

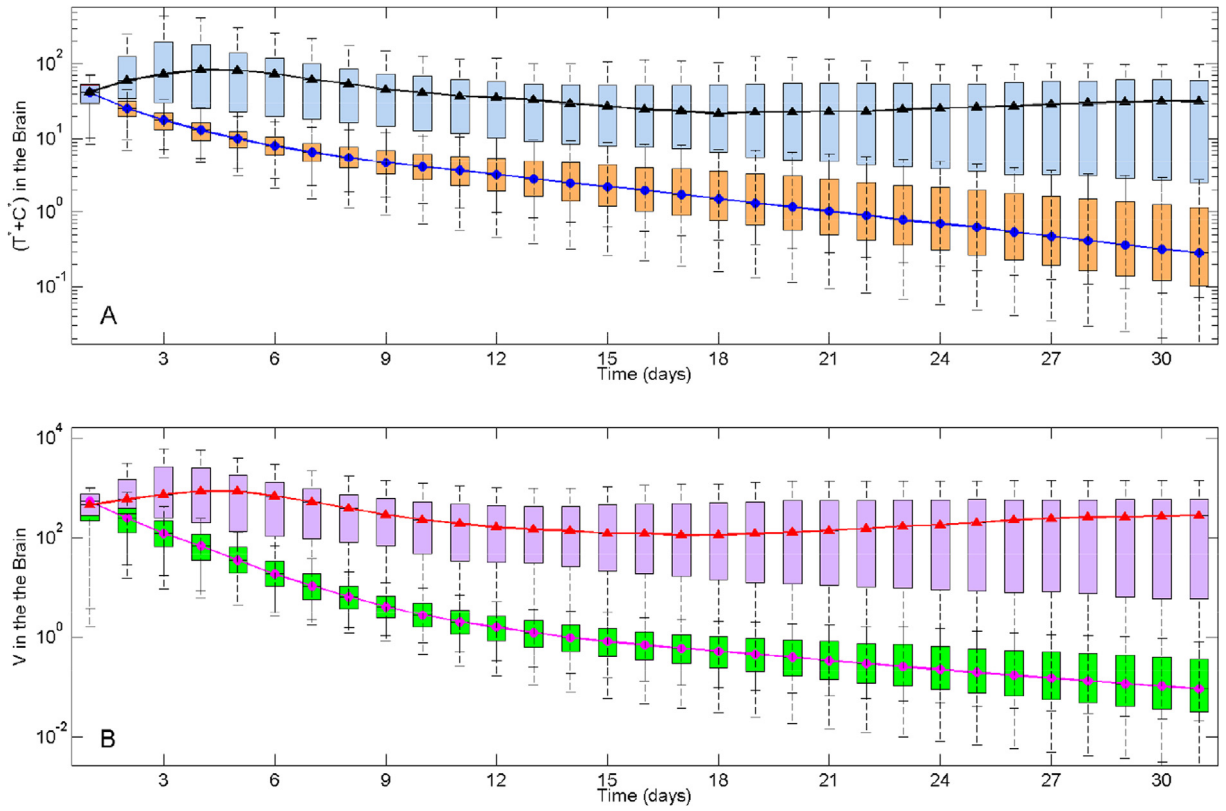

Fig. 3. Comparisons of Scenario B and Scenario C: concentrations of infected T cells ($T^* + C^*$) and HIV virus (V) in the Brain. Each box-plot represents the results of 500 simulations. These plots show median values (solid red circles), upper and lower quartiles, and outlier cutoffs.

Acknowledgments

This study was sponsored by grants from the Natural Science Foundation of China (No. 11271246 and No. 11331009).

Appendix

The dispersal of cells and virus among blood, tissues and the sanctuary (such as the brain) are governed by the rate constants d^T, d^{T^*}, d^{C^*}, d^V and the matrix A. The matrix $A = G - M$ represents the allowed dispersal transitions, where G is the adjacency matrix of the dispersal network, mediating that $G_{ij} = 1$ if cells or virus are allowed to move from patch j to patch i. M represents emigration, and is thus a diagonal matrix with entries $M_{ii} = \sum_{j=1}^{n} G_{ji}$. Here we have neglected the death rates and birth rates of individuals during the dispersal process. So matrix G and M are as follows:

$$G = \begin{bmatrix} 0 & 1 & 1 & \dots & 1 \\ 1 & 0 & 0 & \dots & 0 \\ 1 & 0 & 0 & \dots & 0 \\ \vdots & \vdots & \vdots & \ddots & 0 \\ 1 & 0 & 0 & \dots & 0 \end{bmatrix}, M = \begin{bmatrix} n-1 & 0 & 0 & \dots & 0 \\ 0 & 1 & 0 & \dots & 0 \\ 0 & 0 & 1 & \dots & 0 \\ \vdots & \vdots & \vdots & \ddots & 0 \\ 0 & 0 & 0 & \dots & 1 \end{bmatrix},$$

and matrix A can be defined as follows:

$$A = \begin{bmatrix} -(n-1) & 1 & 1 & \dots & 1 \\ 1 & -1 & 0 & \dots & 0 \\ 1 & 0 & -1 & \dots & 0 \\ \vdots & \vdots & \vdots & \ddots & 0 \\ 1 & 0 & 0 & \dots & -1 \end{bmatrix}$$

In order to find the disease-free equilibrium of system (1), we consider

$$\frac{dT_i}{dt} = \lambda_i - \omega T_i + \sum_{j=1}^{n} d_{ij}^T T_j A_{ij} \tag{2}$$

which can be rewritten as

$$\frac{dT}{dt} = \overline{\lambda} + \Theta T, \tag{3}$$

where $T = (T_1, T_2, \ldots, T_n)^T, \overline{\lambda} = (\lambda_1, \lambda_2, \ldots, \lambda_n)^T$ and the matrix Θ is

$$\Theta = \begin{bmatrix} d_{11}^T a_{11} - \omega & d_{12}^T a_{12} & \ldots & d_{1n}^T a_{1n} \\ d_{21}^T a_{21} & d_{22}^T a_{22} - \omega & \ldots & d_{2n}^T a_{2n} \\ \vdots & \vdots & \vdots & \vdots \\ d_{n1}^T a_{n1} & d_{n2}^T a_{n2} & \ldots & d_{nn}^T a_{nn} - \omega \end{bmatrix}.$$

Obviously, the positive equilibrium of the model (2) exists, denoted by

$$\tilde{T} = \left(\widetilde{T_1}, \widetilde{T_2}, \ldots, \widetilde{T_n}\right) = -\left(\Theta^{-1}\overline{\lambda}\right)^T = -\overline{\lambda}^T\left(\Theta^{-1}\right)^T.$$

It is easy to prove that the positive equilibrium $\tilde{T}$ is globally asymptotically stable if all the eigenvalues of the matrix Θ have negative real parts, i.e. the following:

$$s(\Theta) < 0, \quad s(\Theta) \triangleq max\{Re\xi : \xi \text{ is the eigenvalue of the matrix } \Theta\}$$

holds. Then positive equilibrium $\tilde{T}$ is unique. Therefore, model (1) has a unique disease-free equilibrium $E^0 = (\tilde{T}, 0, 0, 0)$, where **0** represents a n-dimensional zero vector.

The linearisation of the infected classes T^*, C^* and V of model (1) at the disease-free state E^0 can be rewritten in the following form:

$$\frac{dX}{dt} = (F_{E^0} - V_{E^0})X,$$

where

$$X = \left(T_1^*, T_2^*, \ldots, T_n^*, C_1^*, C_2^*, \ldots, C_n^*, V_1, V_2, \ldots, V_n\right)^T$$

and

$$F_{E^0} = \begin{bmatrix} \Omega_1 & \mathbf{0} & \Lambda_1 \\ \mathbf{0} & \Omega_2 & \Lambda_2 \\ N_T\delta\mathbf{I} & N_C\mu\mathbf{I} & \Omega_3 \end{bmatrix}_{3n\times 3n},$$

in which $\mathbf{I}$ is unit matrix of $n \times n$ and

$$\Omega_1 = \begin{bmatrix} 0 & d_{12}^{T^*} & \ldots & d_{1n}^{T^*} \\ d_{21}^{T^*} & 0 & \ldots & 0 \\ \vdots & \vdots & \vdots & \vdots \\ d_{n1}^{T^*} & 0 & \ldots & 0 \end{bmatrix}_{n\times n}, \quad \Lambda_1 = \begin{bmatrix} k_1\widetilde{T_1} & 0 & \ldots & 0 \\ 0 & k_2\widetilde{T_2} & \ldots & 0 \\ \vdots & \vdots & \vdots & \vdots \\ 0 & 0 & \ldots & k_n\widetilde{T_n} \end{bmatrix}_{n\times n},$$

$$\Omega_2 = \begin{bmatrix} 0 & d_{12}^{C^*} & \ldots & d_{1n}^{C^*} \\ d_{21}^{C^*} & 0 & \ldots & 0 \\ \vdots & \vdots & \vdots & \vdots \\ d_{n1}^{C^*} & 0 & \ldots & 0 \end{bmatrix}_{n\times n}, \quad \Lambda_2 = \begin{bmatrix} k_1'\widetilde{T_1} & 0 & \ldots & 0 \\ 0 & k_2'\widetilde{T_2} & \ldots & 0 \\ \vdots & \vdots & \vdots & \vdots \\ 0 & 0 & \ldots & k_n'\widetilde{T_n} \end{bmatrix}_{n\times n},$$

$$\Omega_3 = \begin{bmatrix} 0 & d_{12}^V & \dots & d_{1n}^V \\ d_{21}^V & 0 & \dots & 0 \\ \vdots & \vdots & \vdots & \vdots \\ d_{n1}^V & 0 & \dots & 0 \end{bmatrix}_{n\times n}$$

in which, $k_i = (1-\alpha_i)(1-\varepsilon_i)k$ and $k_i' = \alpha_i(1-\varepsilon_i)k$, $i = 1, 2, \dots, n$.

$$V_{E^0} = \begin{bmatrix} \Phi_1 & \mathbf{0} & \mathbf{0} \\ \mathbf{0} & \Phi_2 & \mathbf{0} \\ \mathbf{0} & \mathbf{0} & \Phi_3 \end{bmatrix}_{3n\times 3n},$$

in which

$$\Phi_1 = \delta\mathbf{I} + \begin{bmatrix} (n-1)d_{11}^{T^*} & 0 & \dots & 0 \\ 0 & d_{22}^{T^*} & \dots & 0 \\ \vdots & \vdots & \vdots & \\ 0 & 0 & \dots & d_{nn}^{T^*} \end{bmatrix}_{n\times n}, \Phi_2 = \mu\mathbf{I} + \begin{bmatrix} (n-1)d_{11}^{C^*} & 0 & \dots & 0 \\ 0 & d_{22}^{C^*} & \dots & 0 \\ \vdots & \vdots & \vdots & \\ 0 & 0 & \dots & d_{nn}^{C^*} \end{bmatrix}_{n\times n},$$

$$\Phi_3 = \sigma\mathbf{I} + \begin{bmatrix} (n-1)d_{11}^{V} & 0 & \dots & 0 \\ 0 & d_{22}^{V} & \dots & 0 \\ \vdots & \vdots & \vdots & \\ 0 & 0 & \dots & d_{nn}^{V} \end{bmatrix}_{n\times n}.$$

Then we found closed forms of R_0 in terms of model parameters using the "next-generation operator" method:

$$R_0 = \rho\left(F_{E^0}V_{E^0}^{-1}\right),$$

where $\rho(F_{E^0}V_{E^0}^{-1})$ is the largest eigenvalue of $F_{E^0}V_{E^0}^{-1}$. Following Theorem 2 in (Van den Driessche and.Watmough, 2002), we have the following result on the local stability of the disease-free equilibrium:

Theorem 1: Let $s(\Theta) < 0$ hold. If $R_0 < 1$, then the disease-free equilibrium E^0 is locally asymptotically stable; If $R_0 > 1$, it is unstable.

The above conclusion shows that, HIV-1 will not be sustained in individual when $R_0 < 1$, otherwise, the infection will approach a positive equilibrium.

References

Bailey, J. R., Sedaghat, A. R., Kieffer, T., et al. (2006). Residual human immunodeficiency virus type 1 viremia in some patients on antiretroviral therapy is dominated by a small number of invariant clones rarely found in circulating CD4+ T cells. *Journal of Virology, 80*(13), 6441–6457.

Barker, C. F., & Billingham, R. E. (1997). Immunologically privileged sites. *Advances in Immunology, 25*(C), 1–54.

Birdsall, H. H., Trial, J., Lin, H. J., Green, D. M., Sorrentino, G. W., Siwak, E. B., et al. (1997). Transendothelial migration of lymphocytes from HIV-1 -infected donors. *Journal of Immunology, 158*, 5968–5977.

Blower, S. M., Gershengorn, H. B., & Grant, R. M. (2000). A tale of two futures: HIV and antiretroviral therapy in San Francisco. *Science, 287*, 650–654.

Burkala, E. J., He, J., West, J. T., Wood, C., & Petito, C. K. (2005). Compartmentalization of HIV-1 in the central nervous system: Role of the choroid plexus. *AIDS, 19*(7), 675–684.

Callaway, D. S., & Perelson, A. S. (2002). HIV-1 infection and low steady state viral loads. *Bulletin of Mathematical Biology, 64*, 29–64.

Davis, L. E., Hjelle, B. L., Miller, V. E., Palmer, D. L., Llewellyn, A. L., Merlin, T. L., et al. (1992). Early viral brain invasion in iatrogenic human immunodeficiency virus infection. *Neurology, 42*(9), 1736–1739.

Frost, S. D., & McLean, A. R. (1994). Quasispecies dynamics and the emergence of drug resistance during zidovudine therapy of HIV infection. *AIDS, 8*(3), 323–332.

Haase, A. T., et al. (1996). Quantitative image analysis of HIV-1 infection in lymphoid tissue. *Science, 274*(5289), 985–989.

Hamed, K. A., Winters, M. A., Holodniy, M., Katzenstein, D. A., & Merigan, T. C. (1993). Detection of human immunodeficiency virus type 1 in semen: Effects of disease stage and nucleoside therapy. *Journal of Infectious Diseases, 167*(4), 798–802.

Hickey, W. F., Hsu, B. L., & Kimura, H. (1991). T-lymphocyte entry into the central nervous system. *Journal of Neuroscience Research, 28*(2), 254–260.

Ho, D. D., Rota, T. R., Schooley, R. T., Kaplan, J. C., Allan, J. D., Groopman, J. E., et al. (1985). Isolation of HTLV-III from cerebrospinal fluid and neural tissues of patients with neurologic syndromes related to the acquired immunodeficiency syndrome. *New England Journal of Medicine, 313*(24), 1493–1497.

Joos, B., Fischer, M., Kuster, H., et al. (2008). HIV rebounds from latently infected cells, rather than from continuing low-level replication. *Proceedings of the National Academy of Sciences, 105*(43), 16725–16730.

Korthals Altes, H., & Jansen, V. (2000). Intra-host competition between nef-defective escape mutants and wild-type human immunodeficiency virus type 1. *Proceedings of the Royal Society B Biological Sciences, 267*(1439), 183–189.

Levy, J. A. (1995). HIV and the pathogenesis of AIDS. *Science, 267*.

Levy, J. A., Hollander, H., Shimabukuro, J., Mills, J., & Kaminsky, L. (1985). Isolation of AIDS-associated retroviruses from cerebrospinal fluid and brain of patients with neurological symptoms. *Lancet, 2*(8455), 586–588.

Lou, J., Lou, Y., & Wu, J. (2002). Threshold virus dynamics with impulsive antiretroviral drug effects. *Journal of Mathematical Biology, 65*, 623–652.

McLean, A. R., & Nowak, M. A. (1992). Competition between zidovudine-sensitive and zidovudine-resistant strains of HIV. *AIDS, 6*(1), 71–79.

Nettles, R. E., Kieffer, T. L., Kwon, P., et al. (2005). Intermittent HIV-1 viremia (Blips) and drug resistance in patients receiving HAART. *Jama the Journal of the American Medical Association, 293*, 817–829.

Nottet, H. S., Van Dijk, S. J., Fanoy, E. B., et al. (2009). HIV-1 can persist in aged memory CD4+ T lymphocytes with minimal signs of evolution after 8.3 years of effective highly active antiretroviral therapy. *Journal of Acquired Immune Deficiency Syndromes, 50*, 345–353.
Nowak, M., & May, R. M. (2001). Virus Dynamics: Mathematical principles of immunology and virology. *Nature Medicine, 410*(6827), 412–413.
Perelson, A. S., Essunger, P., Cao, Y., Vesanen, M., Hurley, A., Saksela, K., et al. (1997). Decay characteristics of HIV-infected compartments during combination therapy. *Nature, 387*, 188–191.
Perelson, A. S., & Nelson, P. W. (1999). Mathematical analysis of HIV-1 dynamics in vivo. *Siam Review, 41*(1), 3–44.
Perelson, A. S., Neumann, A. U., Markowitz, M., Leonard, J. M., & Ho, D. D. (1996). HIV-1 dynamics *in vivo*: Virion clearance rate, infected cell life-span, and viral generation time. *Science, 271*, 1582–1586.
Persaud, D., Siberry, G. K., Ahonkhai, A., et al. (2004). Continued production of drug-sensitive human immunodeficiency virus type 1 in children on combination antiretroviral therapy who have undetectable viral loads. *Journal of Virology, 78*, 968–979.
Ping, L. H., Cohen, M. S., Hoffman, I., Vernazza, P., Seillier-Moiseiwitsch, F., Chakraborty, H., et al. (2000). Effects of genital tract inflammation on human immunodeficiency virus type 1 V3 populations in blood and semen. *Journal of Virology, 74*(19), 8946–8952.
Rong, L., Feng, Z., & Perelson, A. S. (2007). Emergence of HIV-1 drug resistance during antiretroviral treatment. *Bulletin of Mathematical Biology, 69*(6), 2027–2060.
Research in Ph.D Thesis “Intrahepatic Immunity of Malaria” by Mr. Kulachat Sae-Jang of Medical Technology, Mahidol University.
Shen, L., & Siliciano, R. F. (2008). Viral reservoirs, residual viremia, and the potential of highly active antiretroviral therapy to eradicate HIV infection. *Journal of Allergy and Clinical Immunology, 122*, 22–28.
Smith, R. J., & Wahl, L. M. (2004). Distinct effects of protease and reverse transcriptase inhibition in an immunological model of HIV-1 infection with impulsive drug effects. *Bulletin of Mathematical Biology, 66*(5), 1259–1283.
Smith, R. J., & Wahl, L. M. (2005). Drug resistance in an immunological model of HIV-1 infection with impulsive drug effects. *Bulletin of Mathematical Biology, 67*(4), 783–813.
Tachet, A., Dulioust, E., Salmon, D., De Almeida, M., Rivalland, S., Finkielsztejn, L., et al. (1999). Detection and quantification of HIV-1 in semen: Identification of a subpopulation of men at high potential risk of viral sexual transmission. *AIDS, 13*(7), 823–831.
Tang, Y. W., Huong, J. T. J., Lloyd, R. M., Spearman, P., & Haas, D. W. (2000). Comparison of human immunodeficiency virus type 1 RNA sequence heterogeneity in cerebrospinal fluid and plasma. *Journal of Clinical Microbiology, 38*(12), 4637–4639.
Van den Driessche, P., & Watmough, J. (2002). Reproduction numbers and subthreshold endemic equilibrium for compartmental models of disease transmission. *Mathematical Biosciences, 180*, 29–48.
Vernazza, P. L., Eron, J. J., Cohen, M. S., van der Horst, C. M., Troiani, L., & Fiscus, S. A. (1994). Detection and biologic characterization of infectious HIV-1 in semen of seropositive men. *AIDS, 8*(9), 1325–1329.
Wahl, L. M., & Nowak, M. A. (2000). Adherence and drug resistance: Predictions for therapy outcome. *Proceedings of the Royal Society B Biological Sciences, 267*(1445), 835–843.